CrossMark

# Novel visible-light-driven S-doped carbon dots/BiOI nanocomposites: improved photocatalytic activity and mechanism insight

Yajun Wang[1,2], Juan Chen[1], Quan Xu[1], Yan Li[1], Tie Fu[1], Guiyuan Jiang[1,*], Yuming Li[1], Zhen Zhao[1], and Yuechang Wei[1]

[1] State Key Laboratory of Heavy Oil Processing, China University of Petroleum, Beijing, Beijing 102249, China
[2] Jiangsu Collaborative Innovation Center of Atmospheric Environment and Equipment Technology (CICAEET), Nanjing University of Information Science & Technology, Jiangsu Key Laboratory of Atmospheric Environment Monitoring and Pollution Control (AEMPC), Nanjing 210044, China

## ABSTRACT

Developing visible light-driven photocatalyst has been paid a lot of attentions due to the intention of utilizing the solar energy. In this present work, novel visible light-driven S-doped carbon dots (S-CDs)/BiOI composites were synthesized via a facile hydrothermal method and followed by a chemisorption. The S-doped carbon dots were applied in the photocatalytic reaction for the first time and show promising results. The S-CDs/BiOI composite was formed with S-CDs uniformly deposited on the surface of thin BiOI nanosheet. All S-CDs/BiOI composites exhibit higher photocatalytic degradation activities of methylene blue (MB) than pure BiOI, and the optimal modification proportion of S-CDs is 1%. And the S-CDs/BiOI composite also exhibits much higher photocatalytic activities than undoped CDs/BiOI composite. The improved photocatalytic performance of S-CDs/BiOI is attributed to the interfacial transfer of electrons from BiOI to S-CDs, resulting in a more effective charge separation and enhanced photocatalytic activity. For the photocatalytic degradation of MB, the active species trapping experiments indicate that the superoxide radical is the main active species of the S-CDs/BiOI composite. Our results suggest that sulfur doping can further improve the performance of CDs and CDs modification can effectively enhance the photocatalytic activity.

Address correspondence to E-mail: jianggy@cup.edu.cn

## Introduction

Over the past decades, photocatalysis with high oxidation ability and broad compound applicability has attracted extensive scientific interests in environmental remediation [1–3]. Seeking visible light-driven photocatalyst has been paid a lot of attentions due to the intention of utilizing the solar energy. Bismuth-containing materials, such as Bismuth oxyhalides [4–6], $Bi_2WO_6$ [7–9], $BiVO_4$ [10, 11], are of great importance because of their high chemical stabilities and visible light absorption capacity. Bismuth oxyhalides, BiOX (X = Cl, Br, I), with excellent optical properties and unique layer structure have promising application in photocatalysis [4, 5]. Among them, BiOI ($Eg$ = 1.8 eV) has the optimal visible light absorption capacity, which makes it become a more attractive photocatalyst [12, 13]. BiOI is a layered compound crystallize in the tetragonal matlockite structure, which has a crystal structure of $[Bi_2O_2]^{2+}$ slabs interleaved by double slabs of I atoms [12, 14, 15]. BiOI has been applied as good photocatalyst in the degradation of organic compounds, such as dye [16], phenolic compounds [17, 18], and antibiotics [19]. However, the photocatalytic performance of pure BiOI has been limited by the high recombination rate of photogenerated charge carriers, and it is still necessary to find an effective way to improve its photocatalytic performance for practical applications. Therefore, many efforts have been devoted to further enhance the photocatalytic activity of BiOI, such as coupling with other semiconductor [20–23], noble metal deposition [24, 25] and synthesis of different morphologies [12]. Formation of semiconductor heterostructure is an effective way to enhance the photoinduced charge separation efficiency and the photocatalytic performance of BiOI, such as the fabrication of AgI/BiOI [26], graphene/BiOI [27]. Though these heterostructures can partly enhance the photocatalytic activity of BiOI, some key problems are still unsolved. For example, AgI usually suffer from instability during the reaction. Therefore, fabrication of BiOI heterostructure with intimately contact, good stability and excellent charge separation ability is still a challenge.

Materials composed with delocalized conjugated π structures have been demonstrated that they can induce rapid photogenerated charge separation and transfer, which can effectively enhance the photocatalytic performance in a conjugated π structure materials-semiconductor heterostructure [28–31]. As a conjugated π structure material, carbon dots (CDs) are nanosized carbon materials composed of $sp^2/sp^3$ hybridized carbon atoms [32]. CDs have attracted a great deal of scientific interest in many research fields due to their unique photoluminescence, outstanding photostability and optical properties [32–34]. Recently, CDs have emerged as a star material in photocatalysis field due to their nontoxicity, easy fabrication and excellent electron transfer rates [32, 35, 36]. Combined CDs with photocatalysts can form intimately contacted interface with uniform distribution due to the small size and rich functional groups of CDs, which is beneficial to the photogenerated charge separation and the enhancement of photocatalytic activity. It has been reported by Kang and coworkers that a CDs-$C_3N_4$ nanocomposite exhibited an excellent performance for photocatalytic overall water splitting [37]. They also synthesized several CDs/semiconductor composites as excellent photocatalysts in organic pollutants degradation and $H_2$ production [38–42], such as CDs/$BiVO_4$ [38], CDs/$Ag_3PO_3$ [39], CDs/$Cu_2O$ [40] and CDs/ZnO [42]. Zhang et al. [43] also found that CDs modified $TiO_2$ composites presented a higher photocatalytic activity than pure $TiO_2$ under UV–Vis and visible light irradiation. The conjugated π structure of CDs can facilitate the photogenerated charge transfer, and CDs can also act as electron acceptors after photoexcitation. Recently, doping heteroatoms in CDs to further optimize the performance of CDs has attracted a lot of scientific interests [32]. It has been proved that doping sulfur to CDs can induce new pronounced activities, and the electron transfer capability of CDs can be further improved [32, 44]. However, up to now, developing S-doped CDs (S-CDs) modified semiconductor composite for efficient photocatalyst is still rare.

Herein, we reported the first example of S-CDs-modified BiOI nanosheets (S-CDs/BiOI) and exploring the application of these composites in the dye degradation. BiOI nanosheets can deliver a relative fast charge transfer, and S-CDs can work as an electron acceptor to further promote the charge separation and transfer. The dye degradation results indicate that the S-doped CDs modification can effectively improve the photocatalytic performance of BiOI. Moreover, the S-CDs/BiOI composite shows much higher photocatalytic activity than undoped CDs/BiOI composite. The type of active species in the dye degradation can also be manipulated by S-CDs modification. The chemical/physical

properties and synergic effect between S-doped CDs and BiOI were also systematically investigated.

## Experimental

All chemicals with analytical purity were obtained from Sinopharm Chemical Reagent Co., Ltd and were used without further purification.

### Preparation

#### Preparation of BiOI

BiOI was synthesized via a hydrothermal method according to the literature [15]. 20 ml KI aqueous solution was dropped into 20 ml $Bi(NO_3)_3 \cdot 5H_2O$ ethanol solution under continuously magnetic stirring (all the solution were 0.5 mol/L). The solution stirred at room temperature for 1 h; then, the solution was transferred to 50 mL autoclave and maintained at 180 °C for 12 h. The precipitates were collected by centrifugation and then washed with ethanol and distilled water three times. Finally, the precipitates were dried at 80 °C.

#### Preparation of S-CDs/BiOI

S-CDs were synthesized via a hydrothermal method according to the literature [45]. 9 mL sodium citrate solution (0.1 M) and 27 mL sodium thiosulfate were added into a 50 mL autoclave, and the autoclave was maintained at 200 °C for 6 h. After cooling down to room temperature, the S-CDs were filtered with cylinder filtration membrane filter (0.22 μm) and dried by a vacuum freeze drier. The S-CDs were dispersed in DI water to obtain a 1 mg/mL S-CDs solution. 1 g BiOI was dispersed in S-CDs solution and kept stirring for 12 h to prepare the S-CDs/BiOI nanocomposites. S-CDs/BiOI nanocomposites prepared by changing the amount of S-CDs solution of 3, 10, 20 and 30 mL were labeled as S-CDs/BiOI-0.3%, S-CDs/BiOI-1%, S-CDs/BiOI-2%, S-CDs/BiOI-3%, respectively. The obtained samples were washed with water and then dried in an oven at 80 °C overnight.

### Characterization

X-ray diffraction patterns (XRD) were measured on a BRUKER D8 ADVANCE X-ray powder diffractometer by using Cu-Kα (λ = 1.5406 Å) radiation with a Nickel filter operating at 40 kV and 10 mA in the 2θ range of 20°–80° at a scanning rate of 4° min$^{-1}$. The patterns for phase identification were compared with JCPDS reference data. The UV–Vis diffused reflectance spectra (DRS) were characterized on a UV–Vis spectrophotometer (Hitachi U-4100) with the integration sphere diffuse reflectance attachment. It was referenced with $BaSO_4$ as the background. The $N_2$ adsorption and desorption was performed on a Micromeritics ASAP2010 analyzer to measure the Brunauer–Emmett–Teller (BET) surface areas and pore size distribution. The morphologies of the as-prepared samples were obtained on a scanning electron microscopy (SEM, Hitachi SU8010) at an accelerating voltage of 30 kV. And the images of high-resolution transmission electron microscopy (HRTEM) were used to further analyze the morphology of the as-prepared samples by a FEI Tecnai F20 field emission source electron microscope. Scanning transmission electron microscopy (STEM) and energy-dispersive X-ray spectroscopy (EDS) elemental mapping images were also obtained by the FEI F20 electron microscope. The photoluminescence (PL) spectra of the samples were analyzed on a Hitachi F-4500 fluorescence spectrophotometer. X-ray photoelectron spectroscopy (XPS) measurements were taken on a Thermo Fisher K-Alpha instrument, and binding energies were calibrated using the C1$s$ peak at 284.6 eV. The electrochemical experimental results were tested on a CHI 660E electrochemical system with a three electrode system, the as-prepared samples worked as a working electrode, a Pt wire served as the counter electrode, and Ag/AgCl electrode (saturates KCl) worked as a reference electrode. A $Na_2SO_4$ (0.1 mol/L) aqueous solution was used as the electrolyte. Electrochemical impedance spectra (EIS) were recorded at 0.0 V (with reference to the Ag/AgCl electrode). A sinusoidal ac perturbation of 5 mV was applied to the electrode in the frequency range of 0.005–10$^5$ Hz.

### Photocatalytic activity measurements

The photocatalytic activities of the samples were measured by the degradation of methylene blue (MB) in an aqueous solution ($1.5 \times 10^{-5}$ mol/L). A 500 W xenon lamp (Shanghai Bilon Co. Ltd) with a 420-nm cutoff filter was used as the visible light source, and the average light intensity was 50 mW/cm$^2$. The photocatalyst (50 mg) was suspended in 100 mL

aqueous solution of MB. Prior to light illumination, the suspension was stirred for 30 min under the dark to reach adsorption–desorption equilibrium. At given time intervals, 5 ml of suspension was collected and centrifuged using a centrifuge (TGL-18C, Flying Pigeon Centrifuge) at 6000 r/min for 10 min to remove the catalysts. Then, the catalyst-free MB solution was analyzed by recording the absorption band (663 nm for MB) using a UV–Vis spectrophotometer (T6 new century, Beijing PERSEE Co. Ltd). The active species in the photocatalytic degradation process could be investigated by trapping experiment. Ammonium oxalate (AO), isopropyl alcohol (IPA), $KBrO_3$ and $N_2$ were used as hole scavenger, hydroxyl radical scavenger, electron and superoxide radical scavenger, respectively.

## Results and discussion

### Catalyst characterization

S-CDs/BiOI composites were prepared by hydrothermal method and followed by a chemisorption. The XRD patterns of BiOI and various S-CDs/BiOI composites are shown in Fig. 1. All the diffraction peaks of the pure BiOI nanosheet can be exactly indexed to the tetragonal structure (space group: $P4/nmm$ (129), unit cell parameters: a = b = 3.984, and c = 9.128 Å, JCPDS No.01-073-2062) [15]. No impurity peaks can be observed, confirming the high purity of the BiOI. As can be seen from the XRD patterns of S-CDs/BiOI composites, the crystal phase of BiOI was not changed after S-CDs
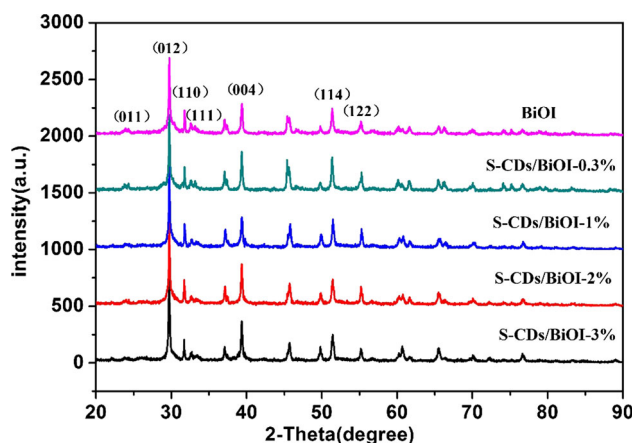


**Figure 1** XRD patterns of BiOI and various S-CDs/BiOI composites.

modification. And no characteristic diffraction peaks of S-CDs can be observed in all S-CDs/BiOI composites, which may be ascribed to the low amount and well dispersion of S-CDs in the composites.

The morphology of BiOI and various S-CDs/BiOI composites is shown in Fig. 2. As can be seen from Fig. 2a, the BiOI nanosheets were successfully synthesized by the hydrothermal method. Figure 2b–d shows the SEM images of S-CDs/BiOI composites with different S-CDs loading amount, after deposited with S-CDs, the morphologies of BiOI nanosheets do not obviously change, which may be due to the small size of S-CDs and the low resolution of SEM characterization.

To further investigate the morphologies of BiOI and S-CDs/BiOI composites, TEM and HRTEM characterizations were performed and the results are shown in Fig. 3. As can be seen, the morphology of BiOI is nanosheet, and the near transparency of the sheets also indicates the ultrathin structure. The measured interplanar spacing is 0.28 nm which corresponds to the BiOI (110) plane. Figure 2c–f shows the HRTEM images of various S-CDs/BiOI composites. It can be seen that the S-CDs are well dispersed on the BiOI nanosheet, indicating the formation of an intimate S-CDs/BiOI heterojunction, which is beneficial to charge separation and transfer. The S-CDs are uniform spherical shape, and the average sizes of S-CDs are around 5 nm. In the enlarged HRTEM image (Fig. 3e), the measured lattice fringe spacing of 0.32 nm is corresponded to the (002) plane of S-CDs, which can also be observed in similar systems [46]. The component of S-CDs/BiOI composite was further studied by the EDS spectroscopy (Fig. S1). Uniform Bi, O, I elements can be observed, which corresponds to the BiOI nanosheet. The C element cannot be investigated due to the carbon background of the carbon support film used in the STEM characterization. The S signal can be found in the S-CDs deposition area, indicating the successful deposition of S-CDs and the doping of S element.

Figure 4 shows the UV–Vis DRS spectra of BiOI and various S-CDs/BiOI nanocomposites. As can be seen, BiOI nanosheet and S-CDs/BiOI composites all exhibit absorption in the visible light range. Pure BiOI presents an absorption edge rise at around 660 nm, corresponding to a band gap of 1.8 eV. After modified with S-CDs, BiOI nanosheets show slightly enhanced light absorption in both UV and visible light range. The band gap energy of all samples can be evaluated by the following equation:
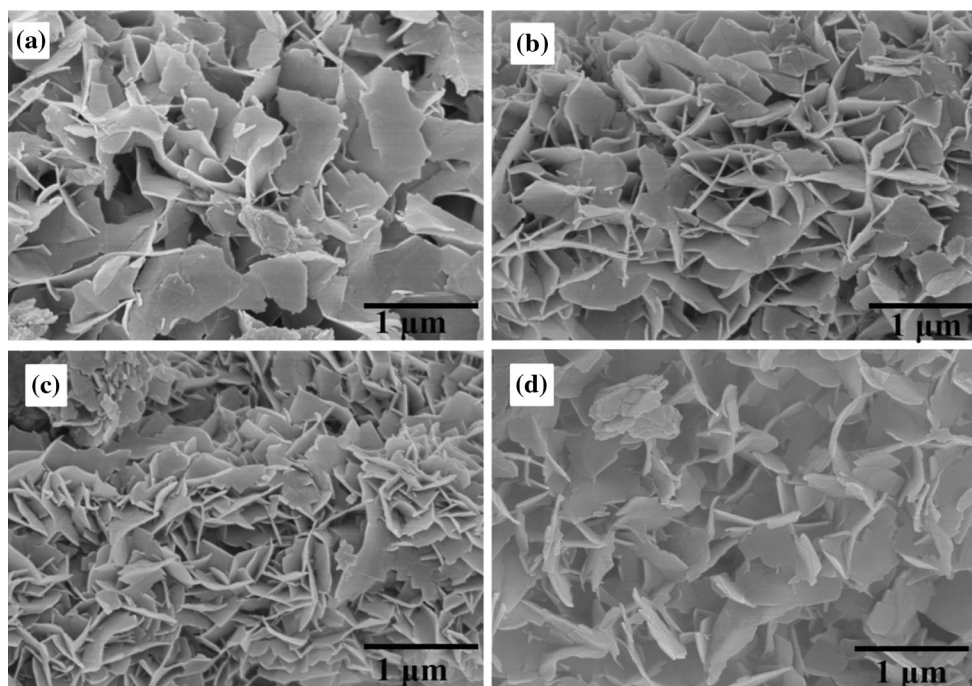
**Figure 2** SEM images of (**a**) BiOI, (**b**) S-CDs/BiOI-1%, (**c**) S-CDs/BiOI-2% and (**d**) S-CDs/BiOI-3%.

$$\alpha h v = A\left(h v - E_g\right)^{n/2} \tag{1}$$

where $\alpha$, $h$, $v$, $A$ and $Eg$ are the absorption coefficient, Planck constant, light frequency, constant and band gap. And the value of n is 4 for BiOI due to the indirect transition. Therefore, the band gap ($Eg$) can be calculated from a plot of $(\alpha h v)^{1/2}$ versus the photoenergy ($hv$) (inset in Fig. 4). The band gap of BiOI and various S-CDs/BiOI nanocomposites were calculated and are shown in Table S1.

The $N_2$ adsorption–desorption experiment was performed to investigate the porosity and surface area of the BiOI and S-CDs/BiOI composite, and the results are shown in Fig. S2. As can be seen, the adsorption–desorption isotherms of BiOI and S-CDs/BiOI-1% almost show no difference. The values of BET-specific surface area and average pore diameter of all samples are listed in Table S1. The BET-specific surface areas of BiOI, S-CDs/BiOI-0.3%, S-CDs/BiOI-1% and S-CDs/BiOI-2% are 9.77, 9.59, 9.09 and 8.89 $m^2$/g, respectively. The specific surface area and average pore diameter of BiOI and various S-CDs/BiOI composites almost show no difference, suggesting that the S-CDs modification would not obviously change the specific surface area and porosity.

The XPS measurement was taken to investigate the chemical states and interaction between BiOI and S-CDs. Figure 5 shows the XPS survey spectra and magnified spectra of Bi 4$f$, I 3$d$, O 1$s$ and C 1$s$. As can be seen, the BiOI and S-CDs/BiOI samples contain Bi, O, I and C. The characteristic peak of S cannot be observed because the peak of S overlaps with that of Bi. In the Bi 4$f$ spectra of BiOI (Fig. 5b), the peaks centered at 159.4 and 164.6 eV are attributed to Bi 4$f_{7/2}$ and Bi 4$f_{5/2}$ of $[Bi_2O_2]^{2+}$, indicating that the Bi atom in BiOI is $Bi^{3+}$ [15]. Two satellite peaks nearby the Bi 4$f_{7/2}$ and Bi 4$f_{5/2}$ main peaks can be observed, which are consistent with the previous reports [14]. The Bi 4$f$ peak in the S-CDs/BiOI composite presents a slight shift when compared to that of pure BiOI. This result implies that the chemical environment of Bi has changed after S-CDs modification and a chemical interaction between the S-CDs and BiOI has formed [47]. As shown in Fig. 5c, in the I 3$d$ spectra of BiOI, two peaks located at 619.2 and 630.6 eV are related to the I 3$d_{5/2}$ and I 3$d_{3/2}$. Compared with that of pure BiOI, the I 3$d$ peaks of S-CDs/BiOI shift to 618.8 and 630.2 eV, which may arises from the coupling of BiOI with S-CDs. In the magnified O 1$s$ spectra of BiOI (Fig. 5d), a broad peak extending from 527.0 to
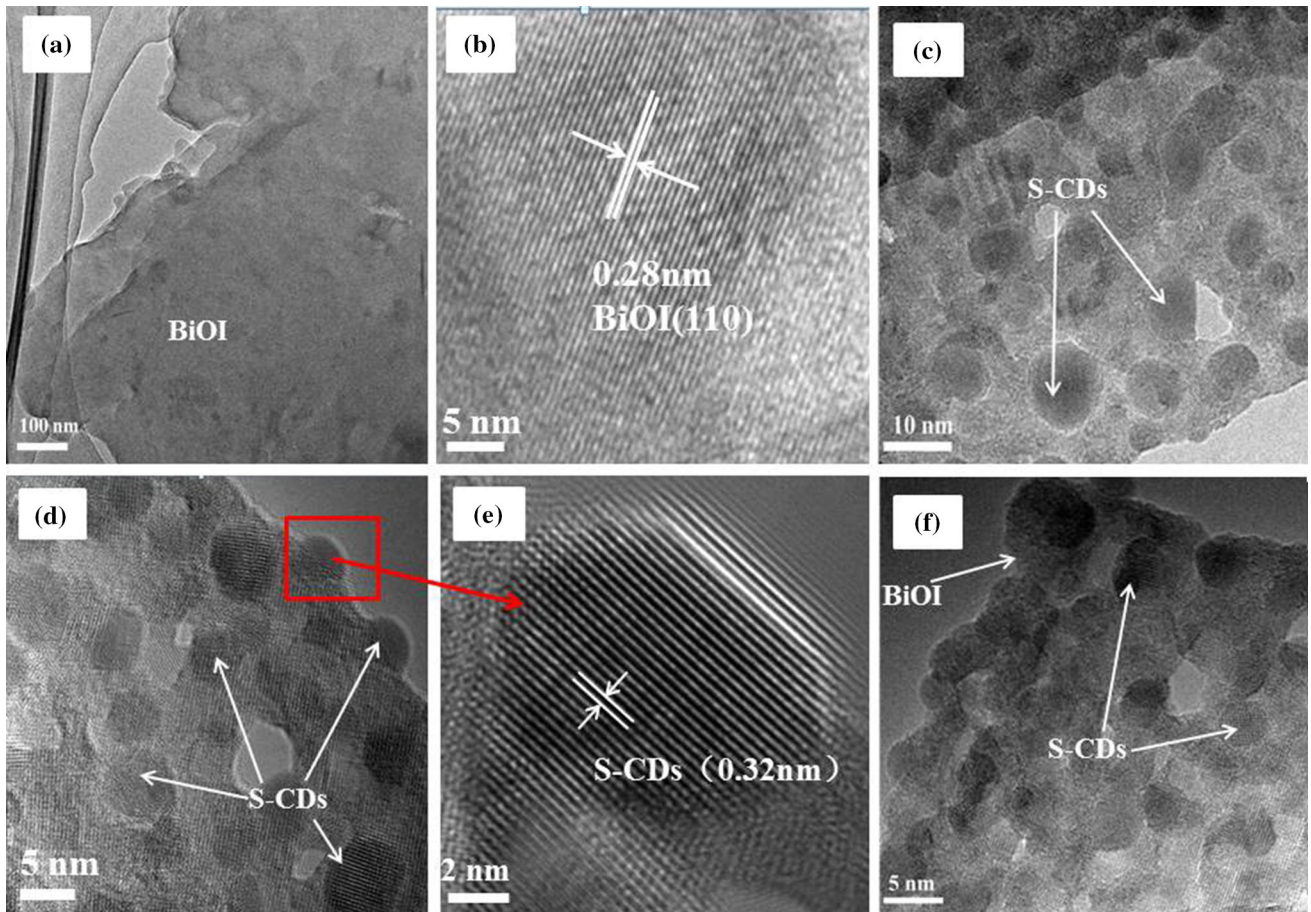
**Figure 3** TEM images of (**a**, **b**) BiOI, (**c**) S-CDs/BiOI-1%, (**d**) S-CDs/BiOI-2%, (**e**) partial enlarged HRTEM image of S-CDs/BiOI-2% and (**f**) S-CDs/BiOI-3%.

535.0 eV can be observed. Two peaks centered at 530.2 and 531.5 eV can be distinguished, which are assigned to the oxygen in BiOI crystals and hydroxyl groups on the surface of the sample [12], respectively.
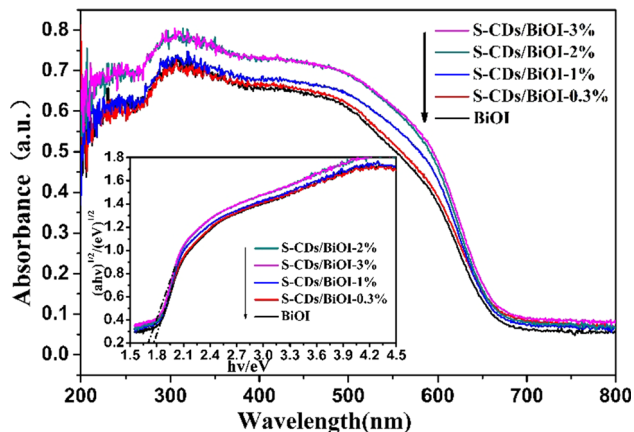


**Figure 4** UV–Vis DRS spectra of BiOI and various S-CDs/BiOI composites.

After modified with S-CDs, the O $3d$ peaks of the BiOI shift to 529.8 and 531.3 eV, respectively. The C $1s$ spectra show two different peaks at 284.6 and 288.7 eV, corresponding to $sp^2$ carbon and C=O [44, 45]. These results imply that there is a chemical interaction between BiOI and S-CDs, which is beneficial to the charge separation and transfer. Moreover, the magnified spectra of S $2p$ of S-CDs are shown in Fig. S3 to further investigate the chemical states of S. The peak centered at 168.0 and 162.0 eV is corresponded to the S $2p_{1/2}$ and S $2p_{3/2}$ [45], indicating the existence of S in the S-CDs. Figure S4 shows the Raman spectra of the BiOI and S-CDs/BiOI-1% composite. Pure BiOI shows one characteristic peak at 150.5 cm$^{-1}$, which attributed to the $Eg$ internal Bi-I stretching mode [48]. The peak of S-CDs/BiOI composite shifts to 152.3 cm$^{-1}$, which further suggests an intensive chemical interaction between BiOI and S-CDs.

**Figure 5** XPS survey spectra of BiOI and S-CDs/BiOI composites (**a**), magnified spectra of (**b**) Bi 4f peaks, (**c**) I 3d peaks, (**d**) O 1 s peaks and (**e**) C 1 s peaks.
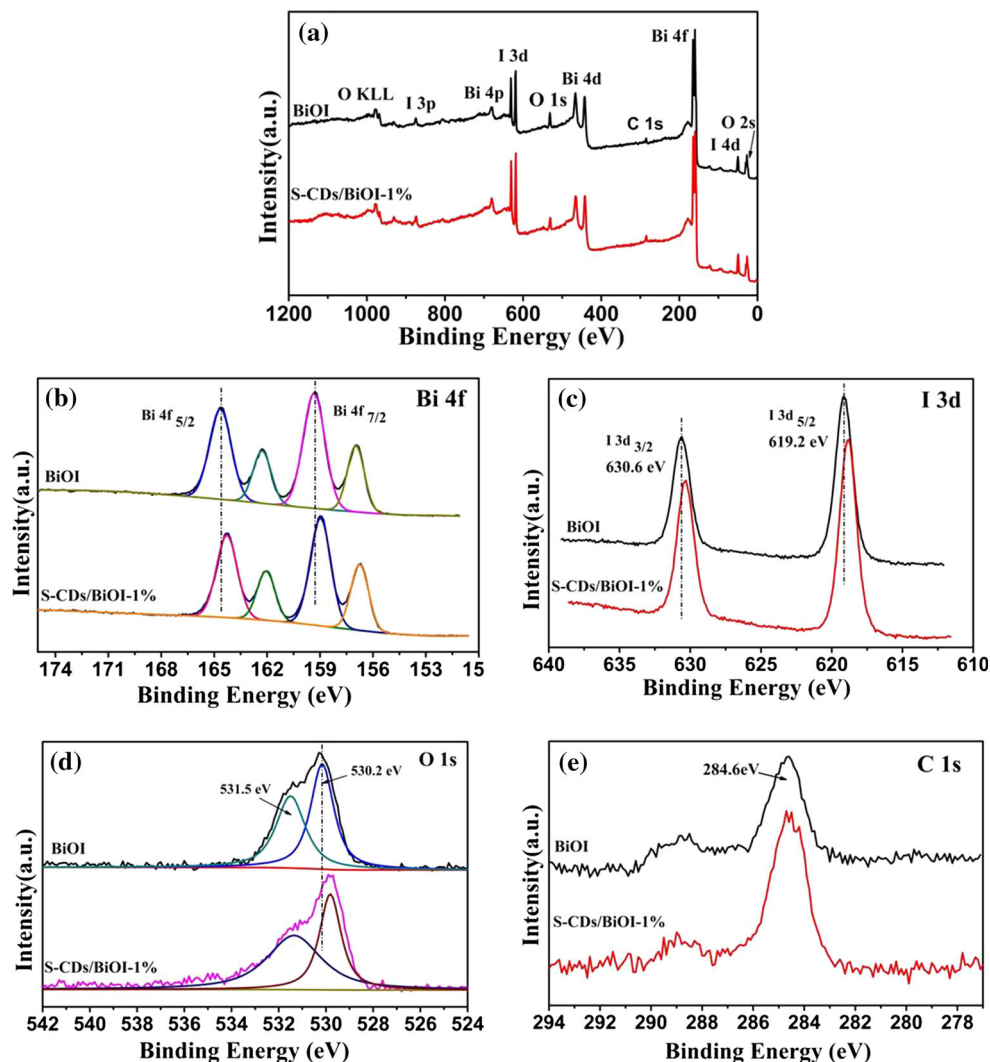


## Enhancement of photocatalytic activity

The photocatalytic activity of BiOI, CDs/BiOI and various S-CDs/BiOI composites was investigated by the degradation of MB under visible light irradiation ($\lambda > 420$ nm), and the results are shown in Fig. 6. As is well known, the photocatalytic degradation processes follow pseudo-first-order kinetics, and the apparent rate constant $k$ of MB degradation over BiOI and various S-CDs/BiOI was calculated and is shown in the insert graph in Fig. 6. The apparent rate constant $k$ of all samples is also shown in Table S2. The visible light photolysis (in the absence of the photocatalyst) of MB was investigated as reference. As can be seen, the visible light photolysis shows a slight degradation of MB. Compared with pure BiOI, all S-CDs/BiOI composites exhibit enhanced photocatalytic activity. The photocatalytic activity of S-CDs/

BiOI first increases then decreases with the increasing amount of the S-CDs. When the proportion of S-CDs reaches 1%, S-CDs/BiOI displays highest photocatalytic activity for the MB degradation. The apparent rate constant $k$ of S-CDs/BiOI is 0.178 h$^{-1}$, which is 76.2% higher than that of pure BiOI. When the proportion of S-CDs exceeds 1%, the photocatalytic activity of S-CDs/BiOI decreases gradually though it still maintains higher than that of pure BiOI. These results imply that the S-CDs modification can effectively enhance the photocatalytic performance of BiOI and there is an optimal modification amount of S-CDs in this composite. Moreover, the pure CDs-modified BiOI was synthesized, and the photocatalytic activity was investigated as reference. The S-CDs/BiOI-1% ($k = 0.178$ h$^{-1}$) exhibits much higher photocatalytic activity than CDs/BiOI-1% ($k = 0.123$ h$^{-1}$), suggesting that doping S element
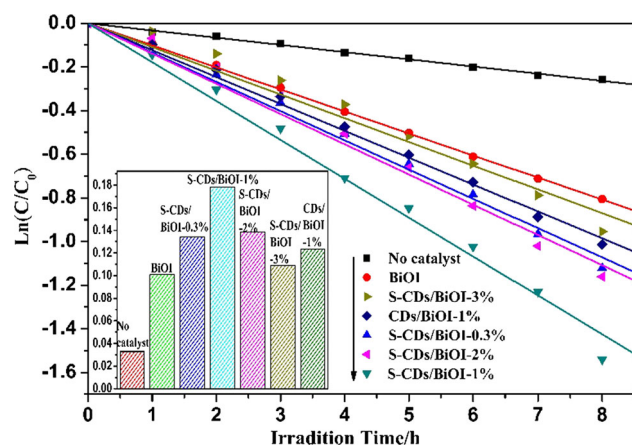
**Figure 6** Photocatalytic activities of pure BiOI, CDs/BiOI and various S-CDs/BiOI composites in the degradation of MB under visible light irradiation (λ > 420 nm), *insert* the apparent rate constant *k* of MB degradation over BiOI, CDs/BiOI and S-CDs/BiOI.

into CDs can further improve the performance of CDs and enhance the photocatalytic activity of BiOI. The recycling experiment was performed to investigate the stability of S-CDs/BiOI composite on MB degradation under visible light irradiation, and the results are shown in Fig. 7. The photocatalytic activity of S-CDs/BiOI could be well maintained after three cycles of MB degradation, revealing that the as-prepared S-CDs/BiOI composite has good photostability.

## Mechanism of enhancement of photocatalytic activity

According to previous reports, organic pollutant adsorption ability, crystal phase structure and separation efficiency of photogenerated charge carriers are crucial factors which affect the photocatalytic activity of photocatalysts [29, 49]. A adsorption equilibrium experiment of pure BiOI and various S-CDs/BiOI composites was performed, and the results are shown in Fig. S5. As can be seen, the adsorption equilibrium could be achieved in 20 min in both the BiOI and S-CDs/BiOI systems. After adsorption equilibrium, 70, 68, 67, 66 and 65% of MB remained in the solution of pure BiOI, S-CDs/BiOI-0.3%, S-CDs/BiOI-1%, S-CDs/BiOI-2% and S-CDs/BiOI-3% composite, respectively. It can be inferred that the pollutant adsorption ability of BiOI was not changed after S-CDs modification. Moreover, based on the XRD patterns (Fig. 1), the crystal structure of BiOI also was not changed after S-CDs modification.

Therefore, the improved charge separation efficiency may be the main factor for the enhancement of photocatalytic activity of S-CDs/BiOI nanocomposite.

Electrochemical impedance spectra (EIS) were obtained to investigate the charge separation efficiency at the interface of BiOI and S-CDs/BiOI composite. Figure S6 shows the EIS Nyquist plots of BiOI and S-CDs/BiOI-1% photocatalysts without and with irradiation. The radius of the arc on the EIS spectra indicates the transfer resistance of charge carriers at the surface of the electrode [7, 50]. As can be seen, the radius of the arc on the EIS spectra of S-CDs/BiOI-1% is smaller than that of pure BiOI under visible light irradiation, revealing that the S-CDs/BiOI-1% has a more effective charge separation and transfer efficiency. Moreover, the S-CDs/BiOI-1% also presents a smaller arc radius on the EIS Nyquist plot than pure BiOI without light irradiation, which indicates that S-CDs modification can change the charge distribution of BiOI and make the charge transfer easier. These results corroborate that the charge separation and transfer efficiency can be improved by forming the S-CDs/BiOI heterojunction. PL measurement is also taken to investigate the charge separation efficiency of BiOI and S-CDs/BiOI composites. The result is shown in Fig. S7. The BiOI shows an emission peak centered at 635 nm, which may corresponds to the near band edge emission of BiOI. After modified by S-CDs, the intensity of emission peak of BiOI decreased obviously, suggesting higher charge separation efficiency of the S-CDs/BiOI-1% sample.

Trapping experiments of radicals and holes were performed to detect the main active species in the photocatalytic process. AO, IPA, $KBrO_3$ and $N_2$ were used as hole scavenger [18], hydroxyl radical scavenger [18], electron and superoxide radical scavenger [51, 52], respectively. As shown in Fig. 8a, a scavenger for superoxide radicals ($N_2$) causes a significant negative influence on the photocatalytic performance, suggesting that the superoxide radicals are main active species of the BiOI system. The addition of AO and IPA both reduce the photocatalytic activity of S-CDs/BiOI in a certain extent, which indicates that hole and hydroxyl radical are part of active species. And the addition of $KBrO_3$ (electron scavenger) only causes a very small change in the photodegradation of MB, indicating that electrons almost do not participate in the reaction. In the S-CDs/BiOI system (Fig. 8b), the photocatalytic activity was greatly prevented by the addition of $N_2$, suggesting that the
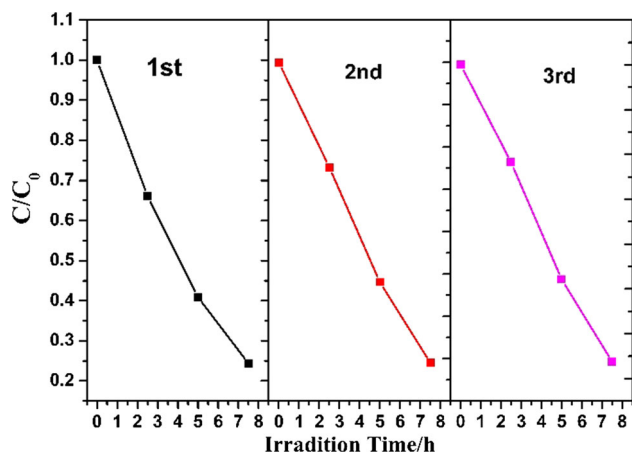
**Figure 7** Recycling test on the S-CDs/BiOI-1% composites for the degradation of MB under visible light irradiation ($\lambda > 420$ nm).

superoxide radicals are main active species of this system. Interestingly and different from pure BiOI, in S-CDs/BiOI system, the electrons can take part in the

degradation of MB in a certain extent. From the above analysis, it can be inferred that the type of active species in the MB degradation can be manipulated by S-CDs modification in BiOI system and the manipulation of active species may achieve different effects in different application.

Based on the aforementioned discussion, the crystal phase structure and the adsorption ability of BiOI were not evidently changed after S-CDs modification. The enhanced photocatalytic performance of S-CDs/BiOI composite may be attributed to the improved charge separation and transfer. A possible photocatalytic mechanism of S-CDs/BiOI composite is presented in Fig. 9. Under the visible light irradiation, BiOI can be excited and generated electron–hole pairs. And S-CDs are good electron acceptor and transporter due to their conjugated π structure, and the excited electrons of BiOI would transfer to the S-CDs [47]. Therefore, an enhanced photocatalytic activity can be achieved by spatial separation of the
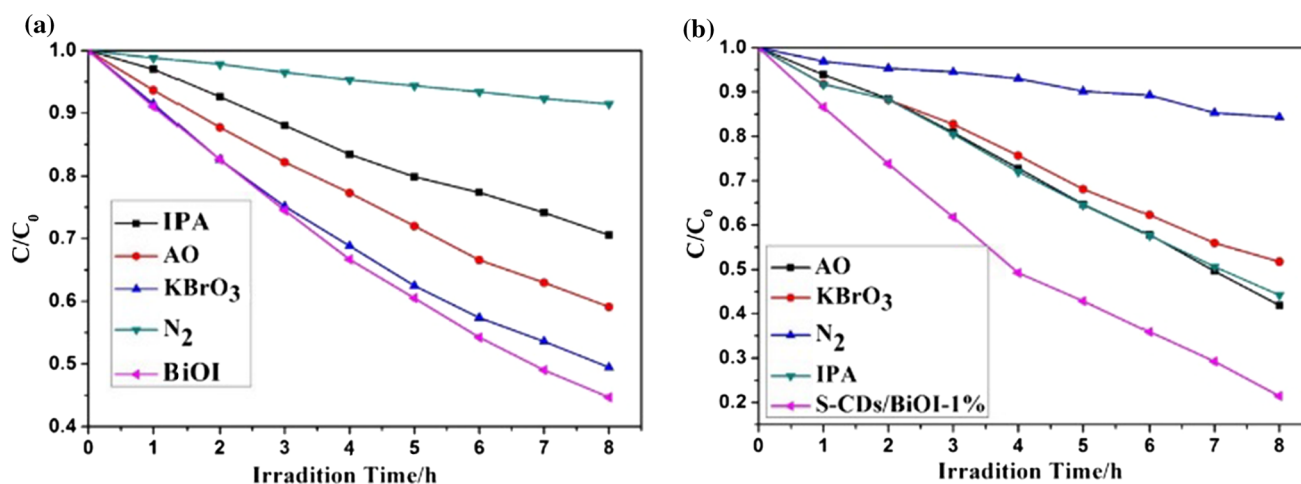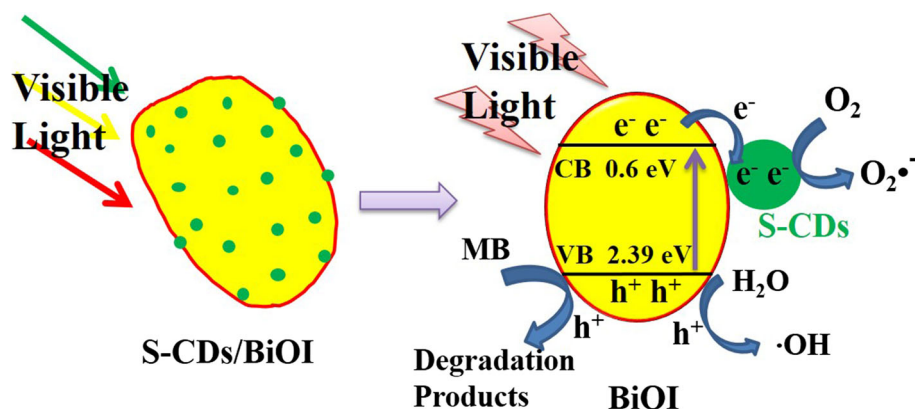


**Figure 8** Ttrapping experiment of active species during the photocatalytic degradation of MB over BiOI (**a**) and S-CDs/BiOI-1% composite (**b**) under visible light irradiation.



**Figure 9** Schematic illustration of the proposed mechanism of S-CDs/BiOI composite.

electron and hole pairs. The electrons would react with oxygen to produce superoxide radicals, and the superoxide radicals play an important role in the degradation of MB in S-CDs/BiOI composite. The holes could oxidize $OH^-$ to yield hydroxyl radical, and the holes and hydroxyl radical also can degrade MB due to their high oxidative capacity. Therefore, the improved photocatalytic performance of BiOI after S-CDs modification can be ascribed to the enhanced charge separation efficiency and transfer.

## Conclusions

A novel S-CDs/BiOI composite has been prepared via a facile hydrothermal method and followed by a chemisorption. S-doped CDs were used to modify BiOI nanosheet for the first time and show promising results. The S-CDs were uniformly dispersed on the surface of BiOI nanosheets, and the intimate S-CDs/ BiOI heterojunction is beneficial to the charge separation and transfer. After modified with S-CDs, the photocatalytic activity of BiOI is obviously enhanced. The S-CDs/BiOI-1% presents the optimal photocatalytic activity which is 76.2% higher than that of pure BiOI. The S-CDs/BiOI nanocomposite also exhibits much higher photocatalytic activity than undoped CDs/BiOI. The enhancement of photocatalytic activity of BiOI after S-CDs modification can be ascribed to the improved charge separation and transfer induced by S-CDs. Moreover, the type of active species in the MB degradation can be manipulated by S-CDs modification in BiOI. Our results may provide a promising way to fabricate highly efficient carbon dots-based photocatalyst.

## Acknowledgement

## Compliance with ethical standards

**Conflict of interest**   The authors declare there is no conflict of interest regarding the publication of this paper.

**Electronic supplementary material:** The online version of this article (doi:10.1007/s10853-017-0965-1) contains supplementary material, which is available to authorized users.

## References

[1] Chen C, Ma W, Zhao J (2010) Semiconductor-mediated photodegradation of pollutants under visible-light irradiation. Chem Soc Rev 39:4206–4219

[2] Wang Y, Wang Q, Zhan X, Wang F, Safdar M, He J (2013) Visible light driven type II heterostructures and their enhanced photocatalysis properties: a review. Nanoscale 5:8326–8339

[3] Hernández-Alonso MD, Fresno F, Suárez S, Coronado JM (2009) Development of alternative photocatalysts to $TiO_2$: challenges and opportunities. Energ Environ Sci 2:1231–1257

[4] Zhang X, Ai Z, Jia F, Zhang LZ (2008) Generalized one-pot synthesis, characterization, and photocatalytic activity of hierarchical BiOX (X = Cl, Br, I) nanoplate microspheres. J Phys Chem C 112:747–753

[5] Dai G, Yu J, Liu G (2011) Synthesis and enhanced visible-light photoelectrocatalytic activity of p–n junction $BiOI/TiO_2$ nanotube arrays. J Phys Chem C 115:7339–7346

[6] Shenawi-Khalil S, Uvarov V, Fronton S, Popov I, Sasson Y (2012) A novel heterojunction BiOBr/Bismuth oxyhydrate photocatalyst with highly enhanced visible light photocatalytic properties. J Phys Chem C 116:11004–11012

[7] Wang Y, Bai X, Pan C, He J, Zhu Y (2012) Enhancement of photocatalytic activity of $Bi_2WO_6$ hybridized with graphite-like $C_3N_4$. J Mater Chem 22:11568–11573

[8] Tang J, Zou Z, Ye J (2004) Photocatalytic decomposition of organic contaminants by $Bi_2WO_6$ under visible light irradiation. Catal Lett 92:53–56

[9] Jaramillo-Páez C, Navío JA, Hidalgo MC, Bouziani A, Azzouzi ME (2017) Mixed $\alpha$-$Fe_2O_3$/$Bi_2WO_6$ oxides for

photoassisted hetero-Fenton degradation of methyl orange and phenol. J Photochem Photobiol A 332:521–533

[10] Kudo A, Omori K, Kato H (1999) A novel aqueous process for preparation of crystal form-controlled and highly crystalline $BiVO_4$ powder from layered vanadates at room temperature and its photocatalytic and photophysical properties. J Am Chem Soc 121:11459–11467

[11] Tokunaga S, Kato H, Kudo A (2001) Selective preparation of monoclinic and tetragonal $BiVO_4$ with scheelite structure and their photocatalytic properties. Chem Mater 13:4624–4628

[12] Ye L, Tian L, Peng T, Zan L (2011) Synthesis of highly symmetrical BiOI single-crystal nanosheets and their 001 facet-dependent photoactivity. J Mater Chem 21:12479–12484

[13] Mera AC, Rodríguez CA, Meléndrez MF, Valdés H (2016) Synthesis and characterization of BiOI microspheres under standardized conditions. J Mater Sci 52:944–954. doi:10.1007/s10853-016-0390-x

[14] Jiang J, Zhang X, Sun P, Zhang L (2011) ZnO/BiOI heterostructures: photoinduced charge-transfer property and enhanced visible-light photocatalytic activity. J Phys Chem C 115:20555–20564

[15] Ding C, Cao F, Ye L, Liu K, Xie H, Jin X, Su Y (2015) Synthesis of $BiOI@(BiO)_2CO_3$ facet coupling heterostructures toward efficient visible-light photocatalytic properties. Phys Chem Chem Phys 17:23489–23495

[16] Wang Y, Deng K, Zhang L (2011) Visible light photocatalysis of BiOI and its photocatalytic activity enhancement by in situ ionic liquid modification. J Phys Chem C 115:14300–14308

[17] Li Y, Wang J, Yao H, Dang L, Li Z (2011) Chemical etching preparation of $BiOI/Bi_2O_3$ heterostructures with enhanced photocatalytic activities. Catal Commun 12:660–664

[18] Li Y, Wang J, Yao H, Dang L, Li Z (2011) Efficient decomposition of organic compounds and reaction mechanism with BiOI photocatalyst under visible light irradiation. J Mol Catal A Chem 334:116–122

[19] Hao R, Xiao X, Zuo X, Nan J, Zhang W (2012) Efficient adsorption and visible-light photocatalytic degradation of tetracycline hydrochloride using mesoporous BiOI microspheres. J Hazard Mater 209–210:137–145

[20] Cao J, Xu B, Luo B, Lin H, Chen S (2011) Novel BiOI/BiOBr heterojunction photocatalysts with enhanced visible light photocatalytic properties. Catal Commun 13:63–68

[21] Li TB, Chen G, Zhou C, Shen ZY, Jin RC, Sun JX (2011) New photocatalyst BiOCl/BiOI composites with highly enhanced visible light photocatalytic performances. Dalton Trans 40:6751–6758

[22] Di J, Xia J, Yin S, Xu H, Xu L, Xu Y, He M, Li H (2014) Preparation of sphere-like g-$C_3N_4$/BiOI photocatalysts via a reactable ionic liquid for visible-light-driven photocatalytic degradation of pollutants. J Mater Chem A 2:5340–5351

[23] Mehraj O, Pirzada BM, Mir NA, Khan MZ, Sabir S (2016) A highly efficient visible-light-driven novel p-n junction $Fe_2O_3$/BiOI photocatalyst: surface decoration of BiOI nanosheets with $Fe_2O_3$ nanoparticles. Appl Surf Sci 387:642–651

[24] Yu C, Yu JC, Fan C, Wen H, Hu S (2010) Synthesis and characterization of Pt/BiOI nanoplate catalyst with enhanced activity under visible light irradiation. Mater Sci Eng B 166:213–219

[25] Yu C, Cao F, Li G, Wei R, Yu JC, Jin R, Fan Q, Wang C (2013) Novel noble metal (Rh, Pd, Pt)/BiOX(Cl, Br, I) composite photocatalysts with enhanced photocatalytic performance in dye degradation. Sep Purif Technol 120:110–122

[26] Chen L, Jiang D, He T, Wu ZD, Chen M (2013) In-situ ion exchange synthesis of hierarchical AgI/BiOI microsphere photocatalyst with enhanced photocatalytic properties. CrystEngComm 15:7556–7563

[27] Huang H, Liu K, Zhang Y et al (2014) Tunable 3D hierarchical graphene–BiOI nanoarchitectures: their in situ preparation, and highly improved photocatalytic performance and photoelectrochemical properties under visible light irradiation. RSC Adv 4:49386–49394

[28] Yu G, Gao J, Hummelen JC, Wudl F, Heeger AJ (1995) Polymer photovoltaic cells-enhanced efficiencies via a network of internal donor-acceptor heterojunctions. Science 270:1789–1791

[29] Wang Y, Shi R, Lin J, Zhu Y (2011) Enhancement of photocurrent and photocatalytic activity of ZnO hybridized with graphite-like $C_3N_4$. Energ Environ Sci 4:2922–2929

[30] Wang Y, Shi R, Lin J, Zhu Y (2010) Significant photocatalytic enhancement in methylene blue degradation of $TiO_2$ photocatalysts via graphene-like carbon in situ hybridization. Appl Catal B Environ 100:179–183

[31] Wang Y, Wang Z, Muhammad S, He J (2012) Graphite-like $C_3N_4$ hybridized $ZnWO_4$ nanorods: synthesis and its enhanced photocatalysis in visible light. CrystEngComm 14:5065–5070

[32] Yu H, Shi R, Zhao Y, Waterhouse GI, Wu LZ, Tung CH, Zhang T (2016) Smart utilization of carbon dots in semiconductor photocatalysis. Adv Mater 28:9454–9477

[33] Xu Q, Zhao J, Liu Y, Pu P, Wang X, Chen Y, Gao C, Chen J, Zhou H (2015) Enhancing the luminescence of carbon dots by doping nitrogen element and its application in the detection of Fe(III). J Mater Sci 50:2571–2576. doi:10.1007/s10853-015-8822-6

[34] Wang J, Qiu J (2016) A review of carbon dots in biological applications. J Mater Sci 51:4728–4738. doi:10.1007/s10853-016-9797-7

[35] Li H, Kang Z, Liu Y, Lee ST (2012) Carbon nanodots: synthesis, properties and applications. J Mater Chem 22:24230–24253

[36] Fernando KAS, Sahu S, Liu Y et al (2015) Carbon quantum dots and applications in photocatalytic energy conversion. ACS Appl Mater Interfaces 7:8363–8376

[37] Liu J, Liu Y, Liu N et al (2015) Metal-free efficient photocatalyst for stable visible water splitting via a two-electron pathway. Science 347:970–974

[38] Tang D, Zhang H, Huang H, Liu R, Han Y, Liu Y, Tong C, Kang Z (2013) Carbon quantum dots enhance the photocatalytic performance of $BiVO_4$ with different exposed facets. Dalton Trans 42:6285–6289

[39] Zhang H, Huang H, Ming H, Li H, Zhang L, Liu Y, Kang Z (2012) Carbon quantum dots/$Ag_3PO_4$ complex photocatalysts with enhanced photocatalytic activity and stability under visible light. J Mater Chem 22:10501–10506

[40] Li H, Liu R, Liu Y, Huang H, Yu H, Ming H, Lian S, Lee ST, Kang Z (2012) Carbon quantum dots/$Cu_2O$ composites with protruding nanostructures and their highly efficient (near) infrared photocatalytic behavior. J Mater Chem 22:17470–17475

[41] Zhang H, Ming H, Lian S, Huang H, Li H, Zhang L, Liu Y, Kang Z, Lee ST (2011) $Fe_2O_3$/carbon quantum dots complex photocatalysts and their enhanced photocatalytic activity under visible light. Dalton Trans 40:10822–10825

[42] Yu H, Zhang H, Huang H, Liu Y, Li H, Ming H, Kang Z (2012) ZnO/carbon quantum dots nanocomposites: one-step fabrication and superior photocatalytic ability for toxic gas degradation under visible light at room temperature. New J Chem 36:1031–1035

[43] Yu H, Zhao Y, Zhou C, Shang L, Peng Y, Cao Y, Wu LZ, Tung CH, Zhang T (2014) Carbon quantum dots/$TiO_2$ composites for efficient photocatalytic hydrogen evolution. J Mater Chem A 2:3344–3351

[44] Qu D, Zheng M, Du P, Zhou Y, Zhang L, Li D, Tan H, Zhao Z, Xie Z, Sun Z (2013) Highly luminescent S, N co-doped graphene quantum dots with broad visible absorption bands for visible light photocatalysts. Nanoscale 5:12272–12277

[45] Xu Q, Pu P, Zhao J, Dong C, Gao C, Chen Y, Chen J, Liu Y, Zhou H (2015) Preparation of highly photoluminescent sulfur-doped carbon dots for Fe(iii) detection. J Mater Chem A 3:542–546

[46] Du QQ, Wang WP, Wu YZ, Zhao G, Ma FK, Hao XP (2015) Novel carbon dots/BiOBr nanocomposites with enhanced UV and visible light driven photocatalytic activity. RSC Adv 5:31057–31063

[47] Di J, Xia J, Ge Y, Li H, Ji H, Xu H, Zhang Q, Li H, Li M (2015) Novel visible-light-driven CQDs/$Bi_2WO_6$ hybrid materials with enhanced photocatalytic activity toward organic pollutants degradation and mechanism insight. Appl Catal B Environ 168–169:51–61

[48] Cao J, Xu B, Lin H, Luo B, Chen S (2012) Novel heterostructured $Bi_2S_3$/BiOI photocatalyst: facile preparation, characterization and visible light photocatalytic performance. Dalton Trans 41:11482–11490

[49] Zhang H, Lv X, Li Y, Li YM, Wang Y, Li JH (2009) P25-graphene composite as a high performance photocatalyst. ACS Nano 4:380–386

[50] Leng WH, Zhang Z, Zhang JQ, Cao CN (2005) Investigation of the kinetics of a $TiO_2$ photoelectrocatalytic reaction involving charge transfer and recombination through surface states by electrochemical impedance spectroscopy. J Phys Chem B 109:15008–15023

[51] Zhu Y, Liu Y, Lv Y, Ling Q, Liu D, Zhu YF (2014) Enhancement of photocatalytic activity for $BiPO_4$ via phase junction. J Mater Chem A 2:13041–13048

[52] Cao J, Li X, Lin H, Chen S, Fu X (2012) In situ preparation of novel p–n junction photocatalyst BiOI/$(BiO)_2CO_3$ with enhanced visible light photocatalytic activity. J Hazard Mater 239–240:316–324